

STATUS REPORT

**ADVANCES IN STEADY- AND UNSTEADY-STATE RELATIVE
PERMEABILITY MEASUREMENTS AND CORRELATIONS**

FY 1995

by

Dan Maloney and Kevin Doggett

July 1995

Work Performed Under Contract No.
DE-AC22-94PC91008

Prepared for
U.S. Department of Energy
Bartlesville Project Office

STATUS REPORT

**ADVANCES IN STEADY- AND UNSTEADY-STATE RELATIVE
PERMEABILITY MEASUREMENTS AND CORRELATIONS
FY 1995**

by

Dan Maloney and Kevin Doggett

Work Performed Under Contract No.
DE-AC22-94PC91008

Prepared for
U.S. Department of Energy
Bartlesville Project Office

DISCLAIMER

This report was prepared as an account of work sponsored by an agency of the United States Government. Neither the United States Government nor any agency thereof, nor any of their employees, makes any warranty, expressed or implied, or assumes any legal liability or responsibility for the accuracy, completeness, or usefulness of any information, apparatus, product, or process disclosed, or represents that its use would not infringe privately owned rights. Reference herein to any specific commercial product, process, or service by trade name, trademark, manufacturer, or otherwise does not necessarily constitute or imply its endorsement, recommendation, or favoring by the United States Government or any agency thereof. The views and opinions of authors expressed herein do not necessarily state or reflect those of the United States Government or any agency thereof.

BDM-Oklahoma, Inc.
P.O. Box 2565

TABLE OF CONTENTS

1.0	INTRODUCTION.....	1
1.1	PROJECT OBJECTIVES.....	1
1.2	PROJECT TASKS.....	2
2.0	UNSTEADY-STATE RELATIVE PERMEABILITY TECHNOLOGY.....	3
2.1	Improvements In Test Automation.....	3
2.2	Unsteady-State Coreflood Tests and Coreflood Simulation.....	5
2.3	Saturation Profile Measurements During Unsteady-State Tests.....	8
3.0	PORE SIZE AND RELATIVE PERMEABILITY CORRELATIONS.....	11
3.1	Sample Selection.....	11
3.2	Comparison of Mercury Capillary Pressure and Oil-Brine Steady-State Relative Permeability Functions.....	11
3.2.1	Steady-State Relative Permeability Tests.....	12
4.0	NON-DARCY FLOW EFFECTS IN MULTIPHASE FLOW SYSTEMS.....	15
5.0	LINEAR X-RAY SCANNER TECHNOLOGY.....	21
5.1	X-ray Terminology and Basic Calculations.....	22
5.2	Incident X-ray Intensities.....	23
5.3	X-ray Detector Output Characteristics.....	24
5.4	X-Ray Calibrations.....	26
5.5	Low Energy X-ray Scans.....	27
5.6	Composite Coreholder.....	27
6.0	EXPLOSION-PROOF OVEN DESIGN.....	29
7.0	TECHNOLOGY TRANSFER.....	31
8.0	OTHER PROJECT ACTIVITIES.....	33
9.0	CONCLUSIONS.....	35
10.0	REFERENCES.....	37

TABLES

4-1	Gas and oil permeability, saturation, and coefficient of inertial resistance results.....	17
5-2	Calculated intensity and throughput results for an aluminum coreholder.	25

FIGURES

2-1	Oil-brine separator/monitor for measuring produced fluid volumes during unsteady-state relative permeability tests.....	4
2-2	Oil-brine relative permeability results for a 259 mD Berea sample. Unsteady-state results were calculated using the Jones-Roszelle (JR) and Welge-Corey (WC) methods.	6
2-3	Oil-brine relative permeability results for 31 mD (ss) and 70 mD (uss) Berea sandstone samples.....	7
2-4	Saturation profiles measured during an oil-brine unsteady-state test on 259 md Berea sandstone.....	8
2-5	Saturation measurements at three positions within the plug of Figure 2-4 plotted as functions of time.....	9
3-6	Mercury injection capillary pressure results for several water-wet sandstone samples...	12
3-7	Imbibition cycle oil-brine relative permeability results for several water-wet sandstone samples.....	12
3-8	Oil-brine relative permeability results for Berea sandstone sample 395-100.	14
3-9	Oil-brine relative permeability results for a Bartlesville sandstone sample.....	14
3-10	Oil-brine relative permeability results for a Bedford Limestone sample.....	14
3-11	Oil-brine relative permeability results for a Bluejacket sandstone sample.....	14
4-12	Pressure drop vs. gas rate for two gas-oil flow ratios.....	18
4-13	Plot to determine the gas permeability and β characteristic for a gas-oil flow ratio(1..	18
4-14	Gas-oil relative permeability results from the data of Table 4-1.....	18
4-15	Correlation between porosity, permeability, and β using the data of Table 4-1.....	18
4-16	Pressure drop vs. oil rate measurements during two-phase gas-oil flow.	19
4-17	ΔP vs. gas rate from 3000	19
4-18	ΔP vs. oil rate from 3000.....	19
4-19	Data results of Figure 4-18 'corrected' according to Equation 4-5	20
5-20	General schematic of the NIPER X-ray source and detector.....	21
5-21	X-Ray results from scans through an aluminum coreholder and Bluejacket sandstone plug.....	23
5-22	X-ray results from scans of aluminum plates.....	24
5-23	Throughput vs. dead-time results for the germanium crystal detector.	25
5-24	Ln (Intensity) vs. NaI concentration for berea sample.	26
6-25	Reservoir condition coreflood schematic. Dimensions are in cm.	29
6-26	Hot oil circulation system	30

ABSTRACT

This report describes the results of tests performed to support development of low-cost, simple methods for estimating fluid transmission characteristics of reservoir rocks; to improve accuracies of laboratory-measured rock fluid transmission characteristics for reservoir engineering designs and recovery predictions; and to provide data and descriptions from multiphase fluid flow tests to support coreflood and reservoir simulator developments.

Conclusions from comparisons of results from both steady- and unsteady-state techniques indicate that experimental techniques and data analysis methods affect results from both methods. A combination of the two techniques provides suitable relative permeability results over the entire range of two-phase flow saturations.

Mercury capillary pressure and oil-brine relative permeability results for a number of water-wet rock samples are compared in this report. The results indicate that both mercury injection and steady-state relative permeability results follow trends related to permeability magnitude in fairly predictable manners. This predictability serves as a basis for goals to provide simple correlations among capillary pressure and relative permeability functions.

Results of a gas-oil two-phase steady-state flow test were evaluated to discern how visco-inertial flow affects both gas and oil production. Visco-inertial gas flow effects influenced both gas and oil production characteristics. A hypothesis was developed to modify the traditional Forchheimer equation that accounts for added flow resistance in multiphase systems.

The hypothesis for treatment of the oil phase under conditions of oil and gas flow when the gas flow is visco-inertial is:

$$-dP / dL - \left[\beta \rho v^2 \right]_{gas} = \left[\mu v / (k_{eff}) \right]_{oil}$$

When the gas velocity is sufficiently low, the second term on the left-hand side of the equation becomes negligible, and the relationship reduces to the familiar Darcy equation. When the gas velocity is such that significant visco-inertial resistance results, the second term on the left-hand side of the equation accounts for this added flow resistance.

A prototype explosion-proof oven in which heat is transferred to the coreflood enclosure by hot silicone oil was tested. The test demonstrated that the hot-oil circulation system is a viable means for heating a coreflood apparatus for reservoir condition tests. A principal advantage of the system is that no ignition sources are present within the enclosure. This is especially important for tests with volatile hydrocarbons because the enclosure can be heated without exceeding the auto-ignition temperatures of the contained hydrocarbons.

EXECUTIVE SUMMARY

The objectives of this project are to improve the reliability of laboratory measurements of multiphase relative permeability at steady- and unsteady-state conditions in core samples; to investigate the influence of rock, fluid, and rock-fluid properties on multiphase relative permeabilities; and to expand the capabilities of measuring relative permeabilities under broader temperature and pressure conditions. Another project objective is to provide low cost methods for estimating relative permeability characteristics when only small reservoir rock samples are available.

Techniques are reported that can be used to improve relative permeability measurements using the unsteady-state coreflood method. An automated system for measuring volumes of oil and brine produced during an unsteady-state coreflood is described. The technique uses radio frequency admittance probes to measure interface levels within oil and brine collection vessels. Using this approach, tens to hundreds of data sets can be recorded during a typical test. Methods for measuring fluid saturation distributions within samples during unsteady-state relative permeability corefloods can be used to provide data sets for coreflood simulation development.

Unsteady- and steady-state oil-brine relative permeability measurements were performed on similar water-wet rock samples to compare results from the two methods. Relative permeability vs. saturation functions were calculated from unsteady-state data using the Jones-Roszelle technique and using a coreflood simulator modeled after the Welge-Corey methods. For the water-wet rock samples tested, the Welge-Corey simulation provided relative permeability results that best matched those of steady-state measurements. Relative permeability vs. saturation functions from the different measurement and data analysis techniques were evaluated. Evaluations focus on differences in brine relative permeability vs. brine saturation functions at low brine saturations for water-wet samples. Primary discrepancies among results were attributed to how data and results are curve fitted and the questionable experimental production data from the unsteady-state test for brine saturations near residual water saturation conditions. Combining results from both steady- and unsteady-state techniques provides suitable relative permeability results over the entire range of two-phase flow saturations.

Laboratory tests were performed to provide data for developing correlations among rock pore size distributions and relative permeability functions. Rock samples were selected from fluvial and beach sedimentary systems for relative permeability, mercury injection, and capillary pressure tests. Samples selected include sandstones from Oklahoma Formations and several samples from the Almond Outcrop G of southwestern Wyoming. Mercury capillary pressure and oil-brine relative permeability results for some of the samples that were previously tested are compared in this report. Results indicate that both mercury injection and steady-state relative permeability follow trends related to permeability magnitude in fairly predictable manners. This predictability serves as a basis for goals to provide simple correlations among capillary pressure and relative permeability functions. Development of reasonably accurate correlations among mercury capillary pressure and relative permeability functions may provide cost effective means for estimating relative permeability functions for rocks when only small samples of the reservoir rock are available. Relative permeability measurements were completed on several water wet sandstone and limestone samples. Other plugs are in various stages of testing.

Results of a gas-oil two-phase steady-state flow test were evaluated to discern how visco-inertial flow affects both gas and oil production. The permeability, porosity, and visco-inertial flow coefficient characteristics measured under two-phase flow conditions follow a correlation that has been reported in the literature for single-phase visco-inertial gas flow. Visco-inertial gas flow effects influenced both gas and oil production characteristics. A hypothesis was developed to modify the traditional Forchheimer equation that accounts for added flow resistance in multiphase systems.

X-ray techniques are used within the scope of this project to measure fluid saturations in rock samples during laboratory tests. The X-ray system and many improvements in linear X-ray scanner operation and X-ray data correlations are described. The non-linearity observed when plotting the natural log of X-ray intensity measurements vs. mass percent of dope included in one of the fluid phases was investigated. It was determined that X-ray calibrations should not be determined based on mass percent of X-ray dope in the flow stream but rather against the volume percent of dope in the flow stream. The literature description that peak detector throughput for a germanium crystal detector occurs for a detector dead-time of about 63% was experimentally verified for the NIPER X-ray detector system. Best linearity in X-ray calibrations against volume percent dope concentrations were achieved with detector dead-times below about 45%. These results were used to determine more efficient ways to obtain X-ray measurements in the laboratory. Peak efficiency is required for measuring quickly moving saturation fronts during rock scans in which a great number of data points are required. Software was written to greatly simplify vertical and horizontal X-ray scanner acquisition and control functions. The two-dimensional X-ray scanner is now fully functional for both single- and dual-energy experiments. Efforts were made to determine the feasibility of using low energy X-ray techniques for rock fluid saturation measurements. A composite material coreholder was purchased to facilitate X-ray measurements of fluid saturations using low energy X-ray scanning techniques.

A prototype explosion-proof oven in which heat is transferred to the coreflood enclosure by hot silicone oil was tested. The heated enclosure maintained the set-point 130°C temperature to within 1°C during a week-long trial. The test demonstrated that the hot-oil circulation system is a viable means for heating a coreflood apparatus for reservoir condition tests. A principal advantage of the system is that no ignition sources are present within the enclosure. This is especially important for tests with volatile hydrocarbons because the enclosure can be heated without exceeding the auto-ignition temperatures of the contained hydrocarbons.

Project members participated in a number of technology transfer activities related to special core analysis measurements. A technical paper describing high-temperature core analysis methods was written. The paper will be presented at the September 1995 Society of Core Analysts International Symposium.

In conclusion, significant progress was made toward meeting objectives of providing low cost, simple methods for estimating fluid transmission characteristics of reservoir rocks; improving accuracies of laboratory-measured rock fluid transmission characteristics, and in providing data and descriptions from multiphase fluid flow tests to support coreflood and reservoir simulator developments. The importance of this work is demonstrated by interest from the petroleum industry.

ACKNOWLEDGMENTS

This work was performed for the U. S. Department of Energy (DOE) under contract DE-AC22-94PC91008. The authors thank Willis Waldorf, Ron Masias, Sam Swan, and Min Tham of NIPER for their assistance in performing this work. We thank the BDM-Oklahoma, Inc. management and personnel who reviewed this manuscript, and Bob Lemmon, DOE Project Manager, for his support.

1.0 INTRODUCTION

The multiphase relative permeability measurement laboratory at NIPER provides a well-used avenue for direct transfer of U.S. Department of Energy supported technology to the oil production industry. The technology developed under this project is available to the petroleum industry for immediate application to increase oil production.

Multiphase relative permeability information is an indispensable component of reservoir simulation for reservoir management and advanced recovery strategies. Under conditions of multiphase flow, fluids such as oil, brine, and gas compete for the same flow paths through the reservoir rock. The additional resistance to flow that occurs when more than one fluid is present in the rock is described by normalizing permeabilities with respect to a base permeability for each of the flowing phases at each fluid saturation condition. This measurement and normalization process yields relative permeability data. Relative permeability characteristics are functions of a number of variables such as the wettability of the rock, the interfacial tensions among the fluids, saturation conditions, hysteresis, and petrographic characteristics of the rock. Laboratory tests are required for these measurements.

Unsteady-state fluid displacement techniques are often used to determine relative permeability characteristics of porous media. Coreflood simulators are being developed to determine relative permeability and capillary pressure vs. saturation functions from unsteady-state test data. Accurate data sets are needed for simulator development. To enhance accuracies of data sets, further development is needed in automating unsteady-state coreflood measurements.

Effective gas permeabilities of porous media are reduced at high gas flow velocities because of visco-inertial flow effects. In multiphase fluid systems, added flow resistance because of visco-inertial gas flow also affects the transmissibility of other fluid phases and is therefore, an important consideration.

Techniques for estimating rock relative permeability characteristics are needed for cases in which plug-size samples are unavailable for laboratory tests. Objectives of this project include development of methods for estimating relative permeability characteristics from capillary pressure measurements on chip-size rock fragments.

Tasks for FY 1995 were planned to improve the reliability of relative permeability measurements and to address Forchheimer effects as well as the influence of pore size distribution on relative permeabilities.

1.1 PROJECT OBJECTIVES

The objectives of this project are to improve the reliability of laboratory measurements of multiphase relative permeability at steady- and unsteady-state conditions in core samples; to investigate the influence of rock, fluid, and rock-fluid properties on multiphase relative permeabilities; and to expand the capabilities of measuring relative permeabilities under broader temperature and pressure conditions. Another project objective is to provide low cost methods for estimating relative permeability characteristics when only small reservoir rock samples are available.

1.2 PROJECT TASKS

Work during the first quarter of FY 1995 continued under FY 1994 work plans. Tasks conducted in FY 1995 include those from both FY 1994 and FY 1995. Project tasks were:

- Perform relative permeability corefloods.
 - Assemble data sets for coreflood simulator evaluation.
 - Provide data to compare with numerical simulator results.
- Investigate Forchheimer effects during steady-state gas-oil or gas-brine relative permeability tests.

Investigators have found significant gas effective permeability reduction when the gas flow velocity is within the visco-inertial regime. Forchheimer effects were measured during steady-state, two-phase gas-liquid flow tests and results were analyzed. It may be important to consider visco-inertial flow effects in both laboratory and field multiphase flow applications.

- Investigate relationships among pore size distributions and oil-brine relative permeability functions.

Often only drill cuttings are available from petroleum formations of interest. This task investigates the potential for estimating relative permeability functions based on measurements on drill cuttings.

- Determine feasibility of using photon spectrum analysis from low energy X-ray scanning to determine fluid saturations in rock samples during laboratory flow tests.
- Interact with industrial sources for technology transfer and to identify technology requirements in special core analysis.

2.0 UNSTEADY-STATE RELATIVE PERMEABILITY TECHNOLOGY

Multiphase relative permeability information is an indispensable component of reservoir simulation for reservoir management and advanced recovery strategies. Relative permeability functions are often determined in a special core analysis laboratory by conducting flow tests on samples of reservoir rocks. For water-wet rocks, oil-brine imbibition cycle relative permeability tests are often performed. These tests provide data which describes relative permeability functions for fluid saturations ranging from residual brine to residual oil conditions. These tests generally fall within two categories; steady-state and unsteady-state measurements. Unsteady-state imbibition tests are performed by injecting brine into a sample containing oil and brine at a residual brine saturation condition. Relative permeabilities are calculated from pressure drop and fluid production data recorded during the test. Steady-state tests are performed by measuring fluid production rates, rock fluid saturations, and pressure drops as brine and oil are injected into the rock. Brine fractional flows (ratio of brine to total oil and brine injection) range from 0 to 1.0 during these tests. The two methods (steady- and unsteady-state) sometimes do not provide identical relative permeability functions.

There is still a great deal of controversy over which method provides data which best represents reservoir processes. Unsteady-state measurements are often favored because of the simplicity of the tests and lower costs compared to steady-state measurements. However, classical unsteady-state methods are unsuited for determining relative permeability functions from low flood rate displacement tests because of the limiting assumptions required for the analyses. The current trend in unsteady-state relative permeability measurement technology is development of techniques to infer relative permeabilities from matching coreflood test data with simulation results. Our project staff generally consider steady-state tests to yield more reliable relative permeability data results compared to those from unsteady-state measurements. Because of the widespread use of unsteady-state data, continuing goals of this project are to develop test methods and analytical techniques which reduce errors from unsteady-state measurements. These goals are focused on improving data acquisition during unsteady-state tests and in providing data for testing unsteady-state coreflood simulators.

2.1 Improvements In Test Automation

One of the greatest challenges in performing an unsteady-state relative permeability tests is to accurately record volumes of produced fluids at appropriate time periods throughout the test. Often, the most important test data results from the early-time portion of the test when rock fluid saturations change rapidly. Typically, manual techniques are employed to record fluid production data during an unsteady-state relative permeability test. Using this method, produced fluids are captured in collection tubes. The test operator must visually monitor volumes of produced fluids at various times during a test. Manual measurement techniques are tedious and prone to error. Furthermore, the number of data points recorded during a test is limited by how quickly the test operator can change fluid capturing tubes and on how much of each fluid must be captured before volumes can be read with the desired accuracy.

Significant efforts were focused during the project year on automating the recording of fluid production data. Because our objectives were also to measure rock fluid saturation distributions during the tests as well as pressure and fluid production histories, automated data logging techniques were required. Also, because X-rays were used for saturation distribution measurements, it was important to isolate the experimental apparatus to minimize exposure of personnel to X-rays.

An automated unsteady-state measurement apparatus was modified and tested. Radio frequency (RF) admittance techniques described in a previous report under this project were used to monitor fluid production during unsteady-state oil-brine tests.¹ Figure 2-1 is a schematic of the coreflood apparatus. An oil-brine separator and a collection vessel are used. The oil-brine separator measures produced oil volumes and the collection vessel measures total volumes of produced fluids. Fluids produced from a core plug during an unsteady-state test are first accumulated in the oil-brine separator. The volume of the tube between the core plug and oil-brine separator is small so that fluids which exit the core plug enter the oil-brine separator as quickly as possible. The time delay between when fluids exit the core plug and enter the separator is accounted when the test results are analyzed. The internal volume within the oil-brine separator is small, so its RF admittance probe accurately registers small changes in oil volumes within the separator. Brine which flows into the oil separator and additional brine displaced from the separator from oil retention flow into the collection vessel. The volume within the collection vessel is larger to accommodate the great volumes of brine injected during a typical test. Brine which accumulates in the collection vessel displaces oil from the vessel. The excess volume within the collection vessel is filled with oil instead of air to prevent the brine from evaporating. Additionally, the RF admittance probe registers oil-brine interface levels with better accuracy than air-brine interfaces.

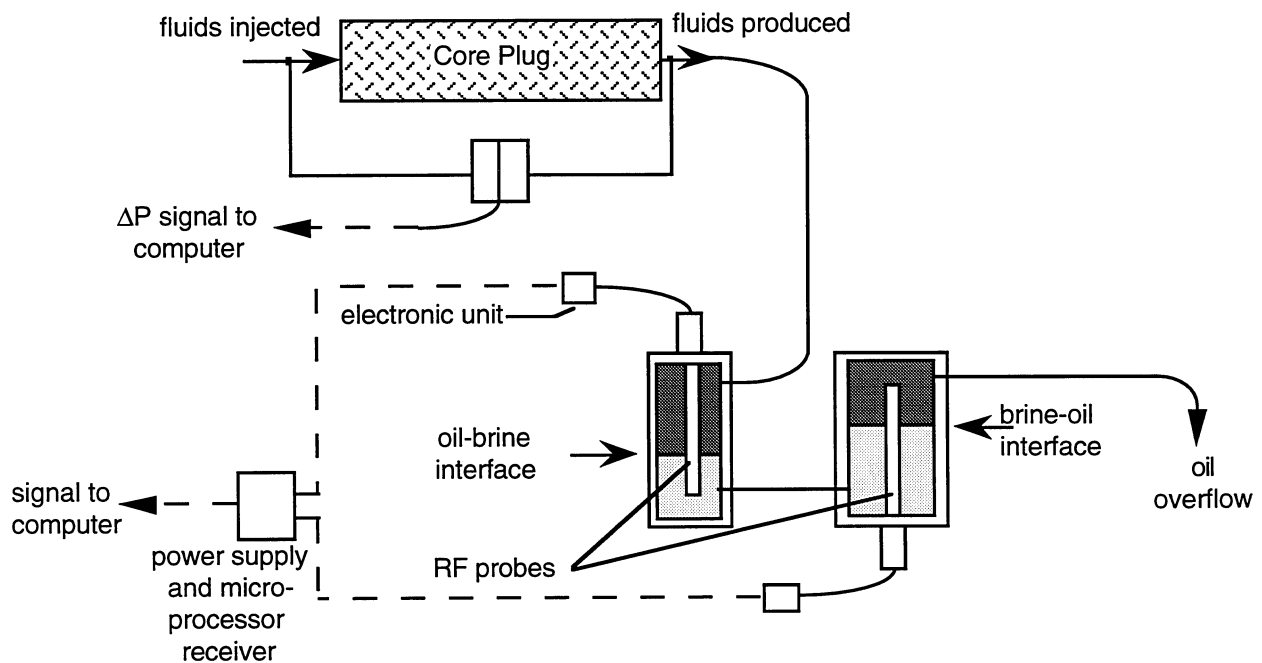


Figure 2-1 Oil-brine separator/monitor for measuring produced fluid volumes during unsteady-state relative permeability tests.

From the two interface measurements and knowing the volumes of each container, the accumulated volumes of oil and brine can be determined at any time during the test. In this manner, tens to thousands of production data points can be easily measured during a typical test. RF admittance probes are available that can be used within pressurized, heated systems. For this reason, the apparatus is suitable for reservoir-condition tests. The only major test constraint using this system is that the brine and oil phases must separate fairly quickly. The system is also suitable with slight modification for oil-displacing-brine tests or for tests in which one of the fluid phases is gas.

2.2 Unsteady-State Coreflood Tests and Coreflood Simulation

An oil-brine unsteady-state relative permeability test was conducted on a Berea sandstone plug to test data logging techniques. The plug was 9.46 cm in length and 3.83 cm in diameter. The pore volume (PV) of the sample was 21.3 cm³. The brine viscosity was of 0.98 cp. The oil viscosity was of 40 cP. Radio Frequency (RF) admittance probes were used to measure volumes of produced fluids during the test.

The permeability of the sample to brine was 259 md. The sample was flooded with oil at a rate of 2 ml/min to a residual brine saturation fraction of 0.261 (26.1% brine saturation). The oil relative permeability at the residual brine condition was 1.5 (150% of the 259 md brine permeability). This oil relative permeability value of 1.5 indicates that the specific permeability of the sample to oil is significantly greater than the brine specific permeability. This condition is not uncommon. Pugh and others reported correlations among air, oil, and brine specific permeabilities (permeabilities when the sample is completely saturated with the injected fluid).² Their correlations were developed from measurements on over 1800 samples from sandstone and carbonate reservoirs (1117 sandstones, 422 dolomites and 329 limestones), covering a permeability range from 0.1 to 10,000 mD. They found that specific permeabilities to oil were slightly lower than the equivalent air permeabilities. The difference was assumed to be primarily from the Klinkenberg effect. The ratio of specific brine to specific air permeability was found, on average, to be about 0.5 over a permeability range from 0.1 to 10,000 mD. This was attributed to the interaction of water with the rock surfaces or clays. Pugh et al. state that significantly larger differences between measured air and brine permeabilities may occur for reservoirs with high concentrations of active clays (at least 5-10% total swelling clays). Correlations from Pugh's work, when applied to a sample of 450 mD air specific permeability, predict an oil specific permeability of about 360 mD and a brine specific permeability of 253 mD. Note that the 360 mD oil specific permeability is about 1.4 times the 253 mD brine specific permeability. For such a sample, it is possible to have oil relative permeabilities, expressed as fractions of brine specific permeabilities, greater than 1 for low brine saturations. This is exactly the case for this Berea sandstone sample. The oil injection rate was adjusted to 0.5 ml/min. The injection fluid was quickly switched from oil to brine to begin unsteady-state test measurements. The plug was X-ray scanned throughout the flood. The X-ray data sets provide information on the movement of fluids through the rock during the test. Fluid production, pressures, and saturation profiles were recorded at time increments until production of oil essentially ceased. Data acquisition techniques were considered successful in recording all pertinent coreflood data. After completing the unsteady-state test, the plug was flooded with oil to a residual brine saturation condition. An imbibition oil-brine steady-state relative permeability test was performed.

Relative permeability results were first calculated using the Jones and Roszelle technique.³ The Jones and Roszelle technique provides results which are similar to those of the Johnson-Bossler-Neumann technique.⁴ Results were also calculated using a coreflood simulator modeled after the Welge-Corey method.^{5,6} Unsteady-state relative permeability results are shown on Figure 2-2. Steady-state relative permeability results are also shown on Figure 2-2 for comparison. The Welge-Corey simulation provided relative permeability results which best matched those of the steady-state measurements.

As shown in Figure 2-2, brine relative permeabilities from the Jones-Roszelle analysis are higher than those from the Welge-Corey and steady-state analyses for brine saturation fractions less than 0.46.

Primary reasons for the discrepancies are attributed to how data and results are curve fitted and the questionable experimental data (from the unsteady-state technique) for brine saturations close to the residual brine saturation condition. With Jones-Roszelle and Johnson-Bossler-Neumann data analysis techniques, there is a direct correspondence between measured data and the relative permeabilities. With the Welge-Corey approach, relative permeability curves result from determining curve fits of exponential form which best fit the data over the range of mobile fluid saturations. The Welge-Corey approach tends to infer the shapes of the relative permeability curves for saturations close to the residual brine saturation condition.

For saturations close to the residual brine saturation condition, how the data are curve fitted has an impact on the resulting relative permeability curves. At the start of an unsteady-state test, immediately after breakthrough of the injected fluid, production rates of each fluid change abruptly. Some of the curve fitting techniques cannot handle abrupt fluid saturation changes. Shown in Figure 2-2 are comparisons of relative permeability results from the Jones-Roszelle method in which two different

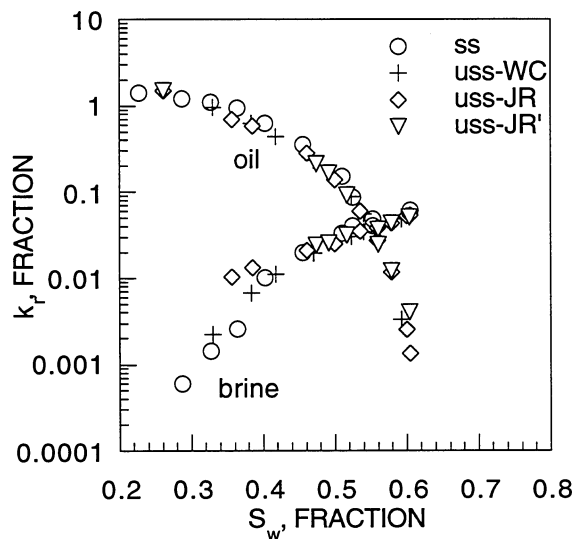


Figure 2-2 Oil-brine relative permeability results for a 259 mD Berea sample. Unsteady-state results were calculated using the Jones-Roszelle (JR) and Welge-Corey (WC) methods. Steady-state (ss) results are also shown for comparison.

techniques were used to fit the experimental data; a least-squares fit (uss-JR) and a Rajan log fit (uss-JR'). In this case, the least-squares and Rajan log fits provide essentially the same relative permeability results, although brine relative permeabilities from the Rajan fit start at a brine saturation fraction of about 0.47, while results using the least-squares fit to the data begin at lower brine saturations.

Figure 2-3 shows additional relative permeability results for two samples of similar permeability. Here, the unsteady-state displacement was piston-like so that the plug end-face saturation changed abruptly immediately following breakthrough of the injected phase (brine).

Although data was recorded at very fine time increments, 15 seconds after breakthrough the end-face brine saturation increased to 55%. This is reflected in the results from the Jones-Roszelle technique. The Jones-Roszelle and Welge-Corey results agree fairly well. Once again, the Welge-Corey technique infers the shapes of the relative permeability curves at low brine saturations even though actual test data was not available in the low brine saturation region. The unsteady-state and steady-state relative permeability results differ, although some of the differences may be attributed to the fact that the tests were not conducted on the same, identical sample.

Reviewing the graphs, it appears that useful information is gained from each relative permeability measurement technique. Combining results from both steady- and unsteady-state techniques provides relative permeability results over the entire range of two-phase flow saturations. This result is consistent with those described by Shafer, Braun, Wood, and Wooten.⁷ In their paper, they describe that neither the steady-state method nor unsteady-state waterflood methods provide relative permeability data at all saturations that exist in an oil/brine reservoir during its productive life. Relative permeability data from the steady-state technique is scarce near the residual oil

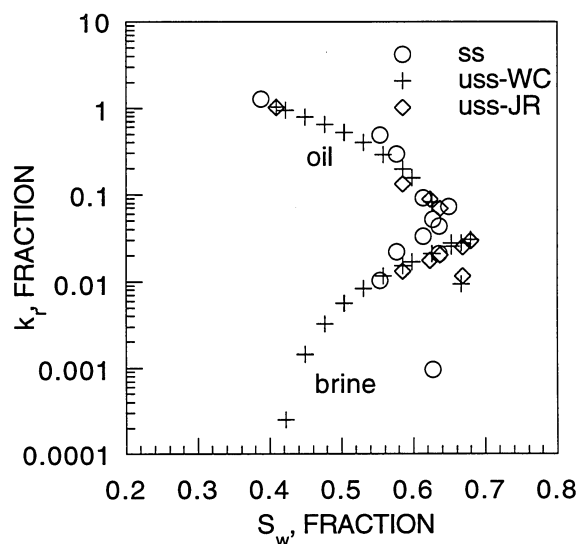


Figure 2-3 Oil-brine relative permeability results for 31 mD (ss) and 70 mD (uss) Berea sandstone samples. Unsteady-state results were calculated using the Jones-Roszelle (JR) and Welge-Corey (WC) methods.

saturation, while data from the unsteady-state technique is generally scarce near the irreducible water saturation. Shafer, Braun, Wood, and Wooten recommend combining steady-state and unsteady-state techniques in a single experiment, providing data over the full range of mobile fluid saturations that otherwise would not be available from either technique separately.

2.3 Saturation Profile Measurements During Unsteady-State Tests

Saturation profiles were measured during the unsteady-state test on the 259 mD Berea sandstone sample. X-ray absorption techniques were used for these measurements. Several of the saturation profiles are shown on Figure 2-4. Bold numbers on the graphs indicate cumulative pore volumes of brine injected into the rock at times when saturation profiles were recorded.

Breakthrough of the brine phase occurred before 0.21 PV of brine was injected. Measurements of saturation profiles at various times during each test provide data which can be used for coreflood simulation.

A reservoir simulator at a minimum should be able to match results from simple laboratory corefloods. An objective for this project is to measure and to report in situ plug saturation histories in addition to data from unsteady-state corefloods. These data can then be used to test simulations. One challenge of this approach is to determine a format for reporting saturation histories so that they are useful for simulation. Saturation distribution results from simulations are essentially snapshots of how fluids are distributed within the rock at specific times.

The X-ray scanner measures saturation profiles of the rock specimens, but the scans themselves take a certain amount of time to complete. For example, data at each scan position illustrated in Figure 2-4 took about six seconds to record. Scanning the rock from inlet to outlet at each of the eight positions took about 48 seconds. For each scan position, time and saturation were recorded.

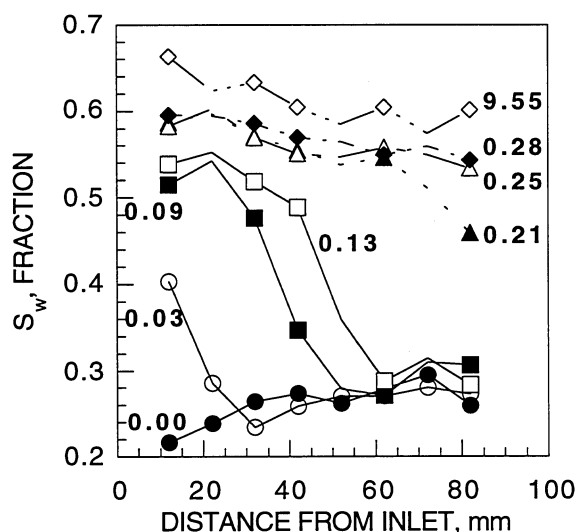


Figure 2-4

Saturation profiles measured during an oil-brine unsteady-state test on 259 md Berea sandstone.

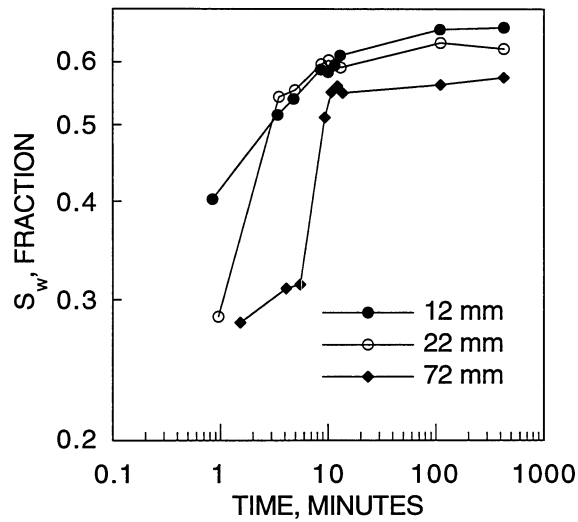


Figure 2-5 Saturation measurements at three positions within the plug of Figure 2-4 plotted as functions of time.

Figure 2-5 shows saturation results for three of the scan positions of Figure 2-4 plotted against time. The measurement at the first point on the curve for a position 12 mm from the plug face was recorded 42 seconds earlier than the first measurement for the point 72 mm from the inlet face of the core plug. When saturations within the rock change slowly, the effect of this time lag is negligible, and the time for the saturation profile can be reported as the average time when the scan data were recorded. For conditions in which saturations change at a faster rate, saturation distributions for the whole sample can be reconstructed for specific times by interpolating from saturation vs. time data for each scan position.

3.0 PORE SIZE AND RELATIVE PERMEABILITY CORRELATIONS

A principal task of this project is to determine relationships among pore size distributions and other rock characteristics and oil-brine relative permeability functions. Often only drill cuttings or small sidewall plugs are available for petroleum formations of interest. This task investigates the potential for estimating relative permeability functions based on mercury injection capillary pressure measurements on small rock samples.

3.1 Sample Selection

Rock samples were selected from fluvial and beach sedimentary systems for relative permeability, mercury injection, and capillary pressure tests. These tests are required to support development of correlations among relative permeability functions and pore size distributions. Selection criteria included the following requirements:

- Samples should be easily obtained or currently available at NIPER.
- Samples should provide a range of permeabilities.
- Samples should be from different sources.
- Samples should exhibit distinct small-scale heterogeneities that are characteristic of generic facies of fluvial or shoreline barrier deposits.
- Data results should be useful to other NIPER groups to maximize project benefits.

Samples were selected from fluvial and beach sedimentary systems. These include outcrop and sub-surface sandstones from Oklahoma Formations and several samples from the Almond Outcrop G of southwestern Wyoming. Additionally, relative permeability measurements were performed on a Berea Sandstone sample to provide data for accomplishing geotechnology research objectives of other Department of Energy funded projects at NIPER.

3.2 Comparison of Mercury Capillary Pressure and Oil-Brine Steady-State Relative Permeability Functions

A primary goal of this project is to relate relative permeability functions to rock pore size and pore shape distribution functions. Mercury injection and other tests are in progress with samples of the rocks for which relative permeability tests have recently been completed. Results for some of the samples that were previously tested (Bentheimer, Berea, Almond formation sandstones) are shown in Figures 3-6 and 3-7. These are only a few of the measurements performed to date on different rock samples. These results indicate that both mercury injection and steady-state relative permeability results follow trends related to permeability magnitude in fairly predictable manners. This

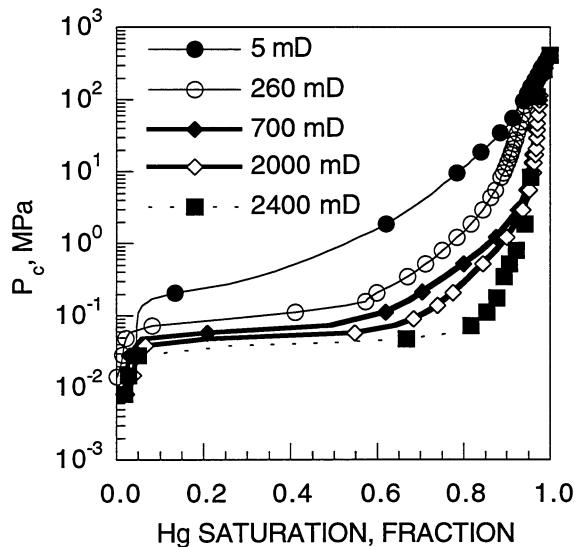


Figure 3-6 Mercury injection capillary pressure results for several water-wet sandstone samples.

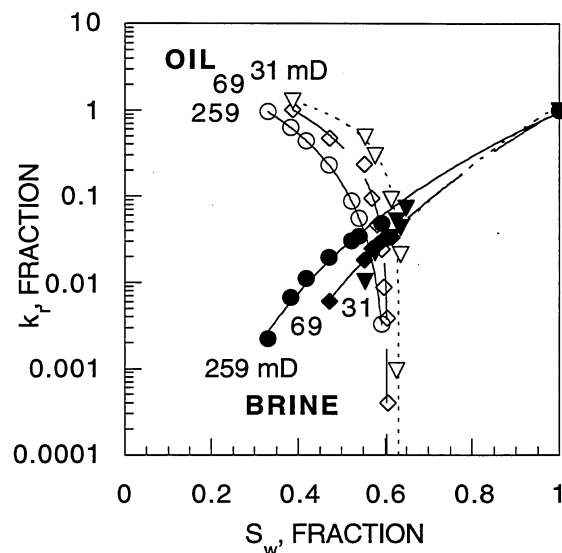


Figure 3-7 Imbibition cycle oil-brine relative permeability results for several water-wet sandstone samples.

predictability serves as a basis to provide simple correlations among capillary pressure and relative permeability functions. Development of reasonably accurate correlations among mercury capillary pressure and relative permeability functions may provide cost effective means for estimating relative permeability functions for rocks when only small samples of the reservoir rock are available. Another incentive for developing such correlations is the cost savings that may be realized in cases where correlations provide adequate accuracies. Mercury injection tests cost several hundred dollars each while steady-state relative permeability tests cost several thousand dollars per test.

To date, progress within this project toward developing correlations among mercury injection and steady-state relative permeability functions has been to collect sufficient data to support future evaluations and analyses. Methods for calculating mercury porosimetry curves using a percolation algorithm for a range of different pore throat and pore size distributions and connectivities have been reported recently.⁸ Other investigators have used these methods to develop 3D network models of porous media. Additional information is being collected on these methods to see how they might simplify development of relative permeability correlations using pore size distribution data from mercury injection measurements.

3.2.1 Steady-State Relative Permeability Tests

Oil-brine, steady-state imbibition-cycle relative permeability tests were completed on several of the rock samples. Berea sandstone, Bartlesville sandstone, and limestone samples were subjected to 5.3 MPa confining pressure during tests. This confining pressure was to insure the fluids injected into rock samples passed through the samples rather than between the samples and rubber sleeves. A Bluejacket sandstone sample was tested with 16 MPa confining pressure. The 16 MPa confining pressure for the

Bluejacket sample was necessary because of the high injection pressures. Flow through the Bluejacket sample was perpendicular to bedding planes.

Tests were performed at the ambient laboratory temperature (23°C). Test fluids were brine and oil. The brine consisted of 6% by weight potassium chloride salt and 8% by weight potassium iodide in deionized water. The brine viscosity was 0.992 cP. Soltrol 100 with 9.2% by weight bromodecane was used as the oil phase. The viscosity of this oil was 1.198 cP. The interfacial tension between the oil and brine was 28 mN/m.

X-ray absorption techniques were used to determine fluid saturation distributions within samples during multiphase flow tests. X-ray calibration procedures were as follows. Initially, each sample was saturated with brine containing only 6% by weight potassium chloride in water. X-ray scans were taken of the sample. For the X-ray tube power settings employed during each test, X-ray absorption results for the core plug when saturated with the 6% potassium chloride looked the same as when saturated only with oil (Soltrol 100 with 9.2% by weight bromodecane). After X-ray scanning the plug in this condition, brine containing 6% potassium chloride and 8% potassium iodide in water was injected into the rock to replace the 6% potassium chloride brine. The sample was then X-ray scanned again. Separate scans of the sample when saturated with these two different brines provided data sets equivalent to 100% oil and 100% brine saturation conditions. These data sets were used to develop correlations between X-ray absorption and oil-brine saturation conditions. Hereafter, the brine containing 6% potassium chloride and 8% potassium iodide in water was used as the test brine.

The following steps were followed for each steady-state relative permeability test. The plug was completely saturated with brine. X-ray response was calibrated for fluid saturation measurements. The permeability of the plug to brine was measured. The plug was flooded with oil to a residual brine saturation condition. The permeability of the sample to oil at the residual brine saturation condition was measured. Relative permeability measurements were recorded with brine fractional flows ranging from 0.01 to 1.0. For most samples, fluid pressure drops were measured across the center section of the sample using taps along the length of the sample that emerged through the side of the coreholder. For samples less than 5 cm long, pressure drops were measured from inlet to outlet plug faces. Fluid saturations were measured using a linear X-ray scanner.

Relative permeability results for samples tested during this reporting period are shown on Figures 3-8 through 3-11. Figures 3-8 and 3-9 show relative permeability results for Berea and Bartlesville sandstone samples. Figure 3-10 shows results for a Bedford limestone sample. Figure 3-11 shows results for a Bluejacket sandstone sample of 0.05 mD brine permeability.

Mercury injection, centrifuge capillary pressure, and thin-section analyses will be performed on samples of these rocks. Data results will be used to support developing correlations among rock pore size distributions and oil-brine relative permeability functions.

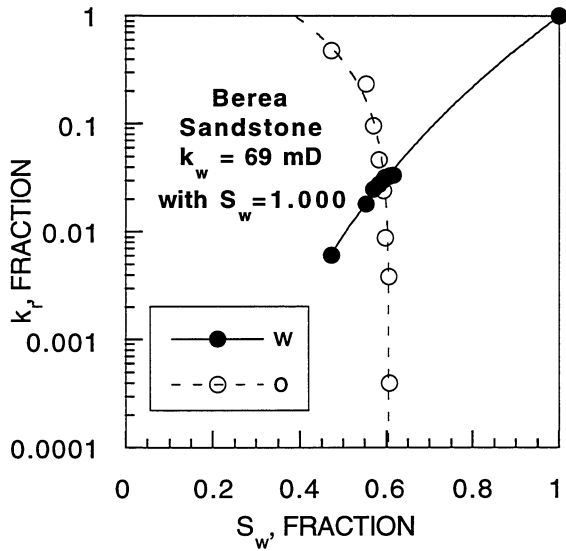


Figure 3-8 Oil-brine relative permeability results for Berea sandstone sample 395-100. Results are normalized with respect to $k_w = 69 \text{ mD}$ with $S_w = 1.000$.

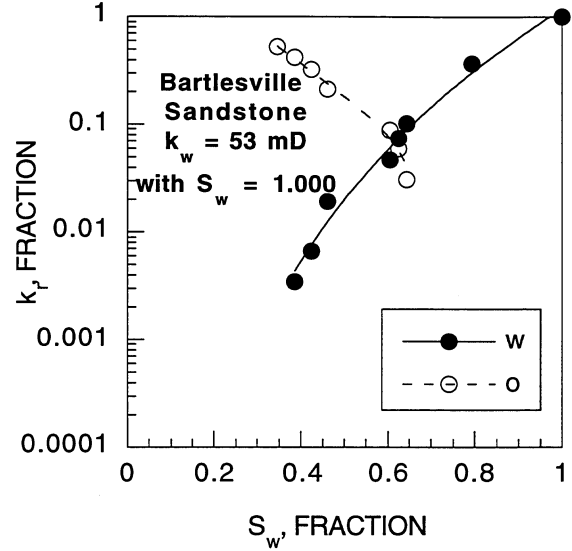


Figure 3-9 Oil-brine relative permeability results for a Bartlesville sandstone sample. Results are normalized with respect to $k_w = 53 \text{ mD}$ with $S_w = 1.000$.

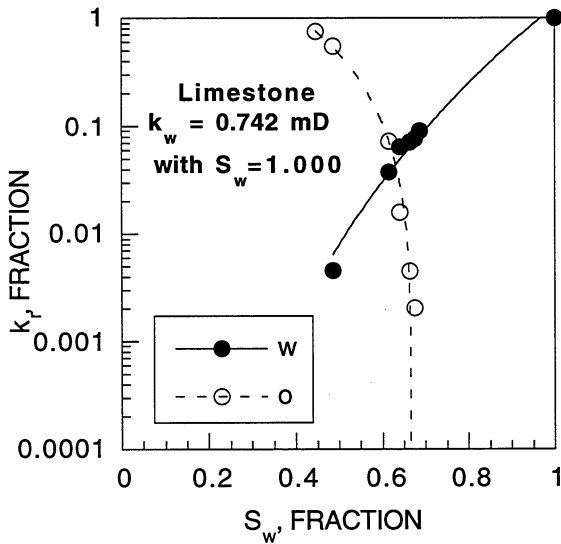


Figure 3-10 Oil-brine relative permeability results for a Bedford Limestone sample. Results are normalized with respect to $k_w = 0.74 \text{ mD}$ with $S_w = 1.000$.

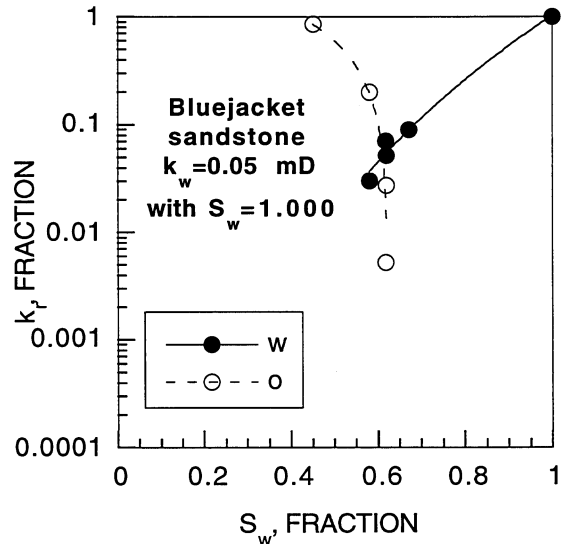


Figure 3-11 Oil-brine relative permeability results for a Bluejacket sandstone sample. Results are normalized with respect to $k_w = 0.05 \text{ mD}$ with $S_w = 1.000$.

4.0 NON-DARCY FLOW EFFECTS IN MULTIPHASE FLOW SYSTEMS

One of the tasks of this project was to evaluate non-Darcy or visco-inertial flow effects on multiphase steady-state fluid flow through rock. Of particular interest in this investigation was how visco-inertial gas flow affects liquid production rates in multiphase gas-liquid flow systems, such as production from condensate reservoirs.

It is well known that pressure gradients are not fully described by Darcy's law when fluids flow through porous media at high velocities.⁹ Results of various studies have been reported describing visco-inertial effects on gas flow systems.⁹⁻²⁵ A generalized equation for linear fluid flow through porous media has been represented by the Forchheimer equation as:^{10,11}

$$-dP / dL = \mu v / k + \beta \rho v^2 \quad (4-1)$$

where P = pressure, atm
 L = length, cm
 μ = viscosity, cP
 v = velocity, cm/s
 k = permeability, darcy
 ρ = density, g/cm³
 β = coefficient of inertial resistance, atm-s²/g

For gases, the equation is often expressed in terms of the mass velocity $W / A = \rho v$ to permit integration. Here, W is the mass flowrate in grams per second, and A is the cross-sectional area in centimeters squared.

Equation 1 reduces to the Darcy permeability equation when flow velocities are such that visco-inertial effects are negligible.

Investigators, including Geertsma and Maloney et al., studied non-Darcy single-phase fluid flow in porous media.^{12,13} Geertsma reported an empirical relationship for determining β for porous media as:

$$\beta \phi^b \sqrt{k} = a \quad (4-2)$$

where ϕ is porosity fraction and β and k are in consistent units to yield a dimensionless result (such as β in cm⁻¹ and k in cm²). Geertsma found constants b and a to be 5.5 and 0.005, respectively. For gas flow cases in which a partial, immobile liquid saturation exists in the porous media, Geertsma suggested using a modified form of Equation 2, which translates to:

$$\beta [\phi(1 - S_L)]^b \sqrt{(k \cdot k_r)} = a \quad (4-3)$$

where k = absolute or reference permeability ($k_{reference}$)
 k_r = relative permeability ($k_{effective} / k_{reference}$, k_{eff} / k)

S_L = liquid saturation (fraction)

A similar result was confirmed in the work of Maloney et al. for single phase gas flow through partially liquid-saturated unconsolidated porous media for a broad range of immobile liquid saturations, although values for b and a were somewhat different than those found by Geertsma. Substituting ϕ_{eff} for $\phi(1 - S_L)$ and k_{eff} for $k \cdot k_r$ yields an equation of the form of Equation 2:

$$\beta \phi_{eff}^{5.5} \sqrt{k_{eff}} = 0.005 \quad (4-4)$$

Here ϕ_{eff} and k_{eff} refer to the fluid phase of interest. ϕ_{eff} represents the pore space occupied by the mobile fluid. In a gas-oil system (with no brine), ϕ_{eff} for the gas phase is $\phi(S_g)$ while ϕ_{eff} for the oil phase is $\phi(S_o)$ where S_g and S_o are the gas and oil saturation fractions.

Two-phase steady-state gas-oil flow measurements were conducted on a 400 md Berea sandstone plug this year to examine visco-inertial flow effects during two-phase flow. Because essentially the same pressure gradient is used to calculate permeabilities for each phase in a multiphase flow system, it was predicted that apparent oil permeabilities would be reduced when gas flow was sufficiently high to cause visco-inertial flow effects.

Tests were conducted with the sample confined within a coreholder. The viscosity of the oil phase was 36.6 cp. Nitrogen was used as the gas phase. The permeability of the sample to gas was measured. Measurements were recorded at low and high gas flow rates so that the visco-inertial flow coefficient could be determined. The sample was saturated with oil. The oil permeability was measured. The plug was flooded with gas to a residual oil saturation condition. Pressure drop and gas rate measurements were recorded with sufficient variations in gas rates to allow determination of the gas permeability and visco-inertial coefficient. Additional gas and oil effective permeability measurements were recorded at gas/oil injection ratios of 3,000:1 and 500:1. For each of the two steady-state flow conditions, pressure drops were recorded for multiple gas and oil injection rates so that gas permeability and β results could be calculated. Particular attention was given to maintaining constant gas/oil injection ratios at each of the two steady-state conditions. This was done so that fluid saturations were essentially constant during each measurement set. Saturations were measured using X-ray attenuation techniques. X-ray results were used to verify that rock fluid saturations remained constant during each set of measurements with a particular fixed gas/oil flow ratio.

Figure 4-12 shows pressure drop vs. gas rate results from measurements when the sample was dry and with a gas-oil injection ratio of 3,000:1. The curvature in each plot appears to result from the added flow resistance from visco-inertial gas flow. Figure 4-13 shows a plot used to calculate the effective gas permeability and β factor for gas flow through the dry rock. Effective gas permeability data and β results were calculated for other gas/oil flow ratios using plots similar to Figure 4-13. Results from each measurement set are shown in Table 4-1. Oil permeability results were calculated from measurements with low gas injection rates. Permeability results were normalized with respect to the oil permeability of the sample (permeability to oil with 100% oil saturation). Relative permeability vs. oil saturation results for both fluid phases are shown in Figure 4-14. Figure 4-15 shows $\beta \sqrt{k_g}$ effective vs. effective porosity (total porosity times gas saturation) for the same data, except that k_g and β units were changed to cm^2 and cm^{-1} , respectively, to yield dimensionless results for $\beta \sqrt{k_g}$. The straight line in Figure 4-15 represents a fit according to Equation 2. As shown by Figure 4-15, Equation 2 appears to provide reasonable correlation among effective porosity, permeability, and the visco-inertial flow

coefficient for multiphase flow, although values for constants b and a are somewhat different than those found by Geertsma.

Table 4-1 Gas and oil permeability, saturation, and coefficient of inertial resistance results

gas/oil flow ratio	$k_{g\text{eff}}$, mD	k_o , mD	S_o , fraction	$\phi_{\text{eff}}(\phi * S_g)$, fraction	β , atm-s ² /g	Comments
1:0	416		0.000	0.220	0.246	dry rock
1:0	289		0.355	0.142	0.601	S _{or}
3,000:1	22	14	0.581	0.092	4.629	2-phase
500:1	25	83	0.684	0.070	11.288	2-phase
0:1		421	1.000	0.000	---	S _o =1.000

Pressure drop vs. oil injection rate results for the two-phase flow measurements are shown in Figure 4-16. Keep in mind that gas was also flowing through the rock as these data were recorded. The gas rate increased with each increase in oil rate to maintain constant gas-oil injection ratios. As gas rates increased, pressure drops increased, which explains curvature in results of Figure 4-16. Applying the Darcy equation to data sets of Figure 4-16 yields oil permeability results that decrease with increasing oil rate, which is incorrect. If such were the case, oil relative permeability vs. oil saturation curves would depend upon gas flow rates. Results from the 3000:1 gas-oil injection ratio are shown for gas and oil phases separately in Figures 4-17 and 4-18. Note that the curvature in pressure drop vs. oil rate results of Figure 4-18 trend in a similar manner to the gas results of Figure 4-17. The apparent added flow resistance, which accompanies oil data of Figure 4-18, results because of visco-inertial gas flow. A correction is needed for the pressure drop vs. oil rate data to account for the added flow resistance because of visco-inertial gas flow effects.

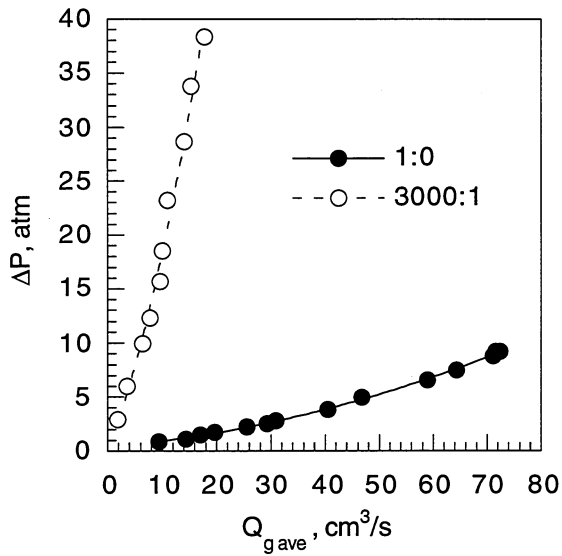


Figure 4-12 Pressure drop vs. gas rate for two gas-oil flow ratios.

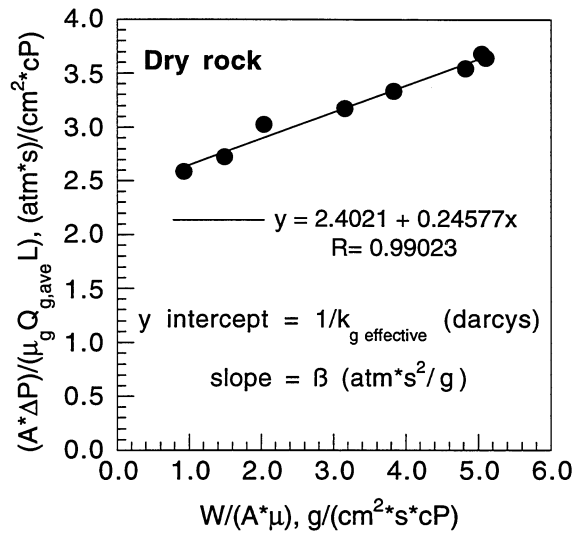


Figure 4-13 Plot to determine the gas permeability and β characteristic for a gas-oil flow ratio (1:0 in this case).

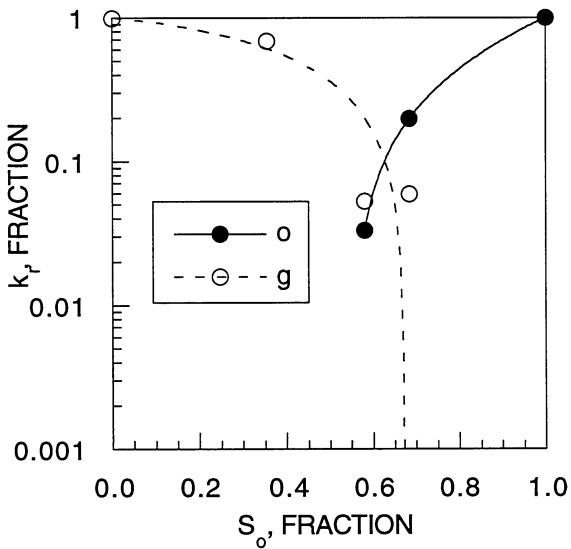


Figure 4-14 Gas-oil relative permeability results from the data of Table 4-1.

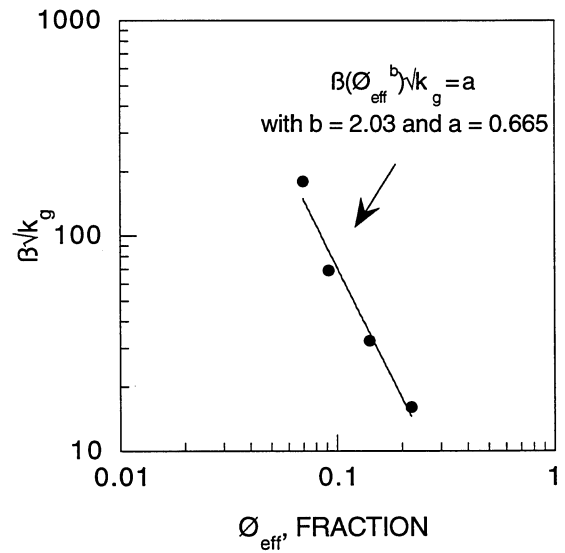


Figure 4-15 Correlation between porosity, permeability, and β using the data of Table 4-1.

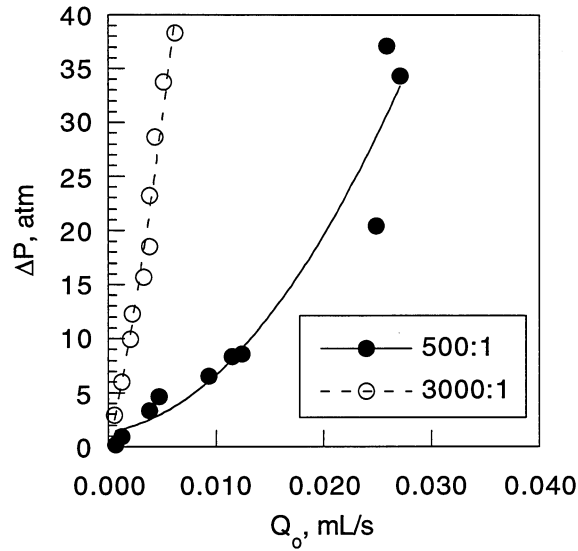


Figure 4-16 Pressure drop vs. oil rate measurements during two-phase gas-oil flow. Results shown are for 500:1 and 3,000:1 gas-oil injection ratios.

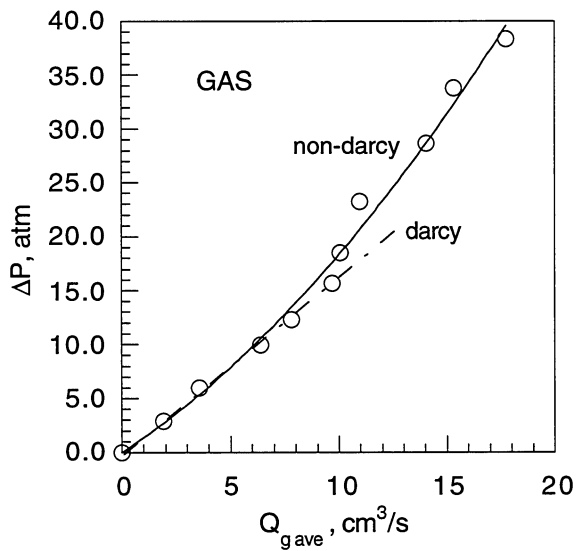


Figure 4-17 ΔP vs. gas rate from 3,000:1 gas-oil ratio measurements.

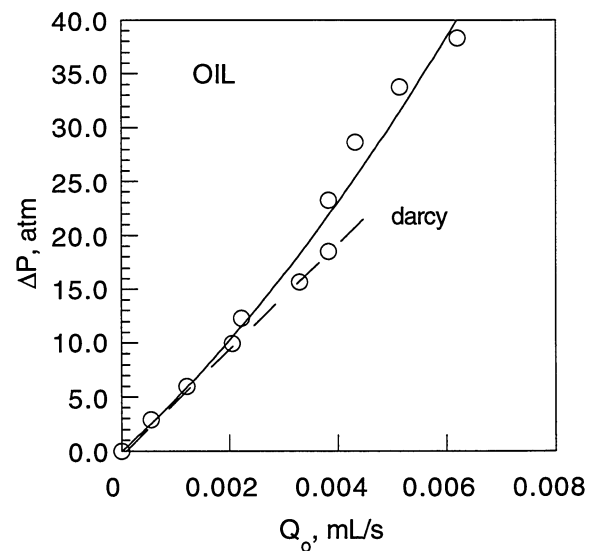


Figure 4-18 ΔP vs. oil rate from 3,000:1 gas-oil ratio measurements.

Considering the results from this test, the following hypothesis for a linear two-phase gas-oil flow system is proposed to account for how visco-inertial flow gas influences oil phase results:

For the oil phase under conditions of oil and gas flow:

$$-dP / dL - \left[\beta \rho v^2 \right]_{gas} = \left[\mu v / (k_{eff}) \right]_{oil} \quad (4-5)$$

When the gas velocity is sufficiently low, the second term on the left-hand side of Equation 4-5 becomes negligible, and the equation reduces to the familiar darcy equation. When the gas velocity is such that significant visco-inertial resistance results, the second term on the left-hand side of equation accounts for this added flow resistance.

Equation 4-5 was tested using the data sets of Figures 4-17 and 4-18. Values of $[\beta\rho v^2]_{gas}$ were calculated from the gas data. Results in Figure 4-18 were 'corrected' by subtracting the visco-inertial gas flow term $([\beta\rho v^2]_{gas})$ of Equation 4-5 from test pressure drops. Results are shown in

Figure 4-19. The dashed line of Figure 4-19 represents the best linear fit to the corrected data from linear regression. This linear relationship indicates that, for the corrected data, the ratio between flow rate and pressure drop is constant. The permeability of the sample to oil for the 3000:1 gas-oil flow ratio can be calculated from the corrected data set using Darcy's law.

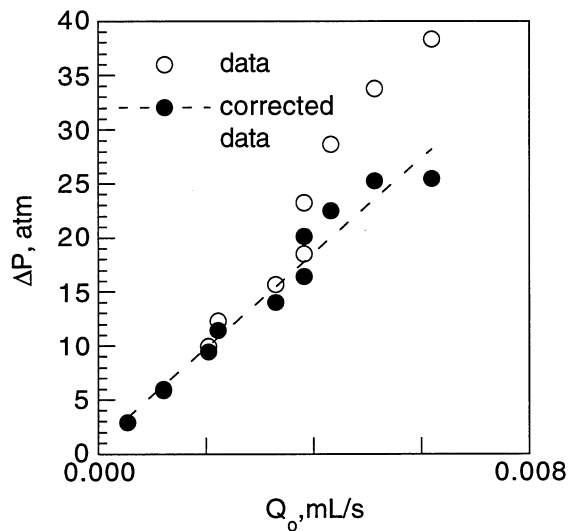


Figure 4-19 Data results of Figure 4-18 "corrected" according to Equation 4-5 to account for visco-inertial gas flow effects

5.0 LINEAR X-RAY SCANNER TECHNOLOGY

Recognition of the need to measure fluid saturation distributions within rock samples during laboratory coreflood tests has increased in recent years. Recently, several personnel from petroleum companies and core analysis laboratories have expressed interest in linear X-ray scanning technology. A linear X-ray scanner is used for various tasks within this project to determine fluid saturation distributions in rock samples during special core analysis tests. Extensive improvements have been made to the scanner in recent years. The purpose of this section is to describe the present configuration of the scanner.

Samples to be scanned are mounted on a stationary track in the center of the X-ray scanning table. The X-ray tube and detector are mounted on a platform which moves under computer control. The scanner can be used for both vertical and horizontal scans. The horizontal scan range is approximately 3 meters while the vertical scan range is approximately 0.6 m. Scan increments can be adjusted according to the nature of the test. For small rock samples, scan increments of 0.1 to 0.5 cm are often employed.

Figure 5-20 is a general schematic of the test arrangement showing the relative position of the sample with respect to the NIPER X-ray source and detector.

The X-ray source is a Philips PW2184/00 tungsten target X-ray spectrophotometer tube, which is rated for 3 kW, 100 kV. The tube is powered by a Philips XRG 3100 X-ray generator, which provides tube voltage from 25 to 60 kV with currents to 80 mA. The X-ray detector is a Canberra low energy germanium detector (GL2020R), which has a 2000 sq. mm area, 20 mm thickness, 0.5 mm Beryllium window, and the following resolution characteristics: FWHM at 5.9 keV of 400 eV and FWHM at 122 keV of 700 eV. The detector has an RC preamplifier. The detector electronics are cooled by liquid nitrogen using a Canberra model 7905-15SL slimline 15 liter, horizontal integral slim line cryostat. Signal processing is by a Canberra Model 1510 integrated signal processor and model 840633 B slave board along with Genie PC basic spectroscopy software for multi-channel data acquisition and analysis. Parker Compumotor indexers and motors along with other hardware are used to control horizontal and vertical movement of the scanning platform.

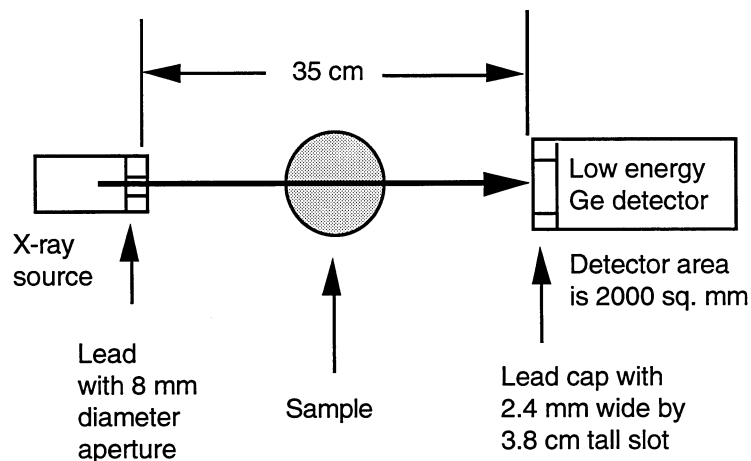


Figure 5-20 General schematic of the NIPER X-ray source and detector.

The detector is surrounded by a Canberra Model 717 detector shield. A thick lead cap was installed into the end of the detector shield between the detector and sample. The lead cap contains a slot that limits X-rays which reach the detector to only those passing through the rock sample. The slot is used to gain better resolution of position-specific X-ray intensities. The multi-channel analyzer and software require a fast computer. A 486 computer is used for this purpose.

Computer programs for X-ray data acquisition and data interpretation were refined during this reporting period. Efforts were concentrated toward simplifying acquisition and control functions during scans of rocks in two dimensions (horizontal and vertical). The National Instruments LabVIEW data acquisition and control program is used for data acquisition functions and to control the X-ray scanner. The LabVIEW computer software accesses the Canberra Accuspec B multichannel analyzer board of the X-ray detector. LabVIEW is used for X-ray measurements so that all data acquisition and control can be done without having to switch back and forth among several different applications. A computer subroutine was written that permits running the DOS-based Accuspec Basic Spectroscopy software of the Canberra germanium crystal detector within LabVIEW (the authors appreciate the contribution of Daryl Doughty, NIPER for writing the subroutine). The Compumotor indexers controlling the horizontal and vertical stages of the X-ray scanner were daisy-chained so that commands to change the scanner horizontal and vertical positions are sent through a single communication channel. Several subprograms controlling different aspects of the automation and data acquisition were written using LabVIEW. These were combined into a main X-ray program. Care was taken to make the program fully modular so that enhancements can be readily added as needs arise. These efforts greatly simplify vertical and horizontal X-ray scanner acquisition and control functions.

5.1 X-ray Terminology and Basic Calculations

X-ray measurements described in following sections of this report are for various X-ray tube voltage and current settings. Because the X-ray source is polychromatic, X-rays with a range of photon energies are emitted from the X-ray tube for particular X-ray generator settings. For this reason, the X-rays which pass through the sample and reach the detector cover a range of photon energies.

Figure 5-21 shows X-ray photons that passed through a coreholder for various tube voltage and current settings. A fairly broad band of X-rays pass through a sample during a typical X-ray scan. For example, for scans of Figure 5-21 with the X-ray generator set to 55 kV, intense X-rays were within a range from about 40 keV to 60 keV with greatest intensity at around 55 keV. Increasing the tube voltage shifts the region of greatest intensity to a higher photon energy and increases the relative intensities of the photons which emerge from the coreholder. Increasing the tube current while keeping the voltage constant generally increases the amplitude of the photon distribution plot. Another way to increase the intensities of detected X-ray photons is to increase the dimensions of the slot within the lead cap in front of the detector. Decreasing the slot size decreases the intensities of detected photons but provides a better measure of the photons which pass through a specific region of the sample.

The X-ray detector is used to count the number of photons which emerge from the coreholder over a specified live-time interval (part of the total detector time is dead-time). Intensities are calculated by dividing the number of counts by the live-time interval in seconds.

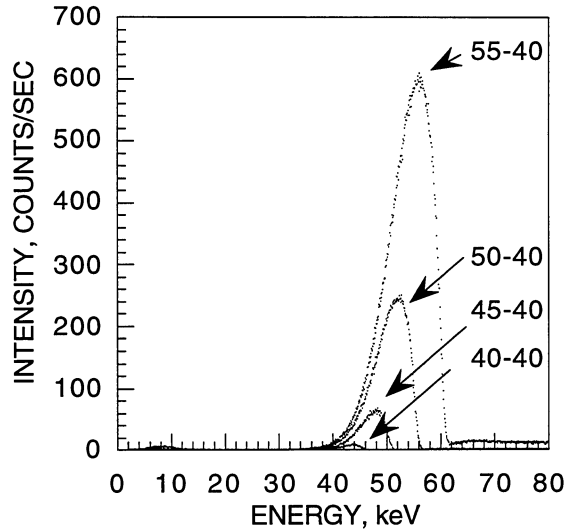


Figure 5-21 X-Ray results from scans through an aluminum coreholder and Bluejacket sandstone plug. X-ray generator kV and mA settings (kV-mA) are shown from scans with different tube voltages.

Lambert's Law is often cited to relate intensities of X-rays which emerge from a sample to intensities of X-rays which are incident to the sample:

$$I = I_0 e^{-kx} \tag{4-6}$$

where I is the emergent intensity, I_0 is the incident intensity, k is the linear absorption coefficient of the sample, and x is the sample thickness. Taking natural logs of both sides of Equation 6 and manipulating yields:

$$\ln(I) = -kx + \ln(I_0) \tag{4-7}$$

For a specific rock sample, the X-ray absorption characteristics of the specific rock and coreholder assembly, and the X-ray path length are constant so that changes in $\ln(I)$ result from changes in rock fluid saturations. X-ray scan results from this laboratory are usually described using natural logs of emergent X-ray intensities because this is the variable predominantly used for rock fluid saturation calculations.

5.2 Incident X-ray Intensities

As long as incident X-ray intensities remain constant throughout a particular flow experiment in which X-ray absorption techniques are used for fluid saturation measurements, a value for the incident intensity is not specifically required. However, knowledge of incident X-ray intensities is important when predicting X-ray absorption characteristics of experimental fixtures that have never

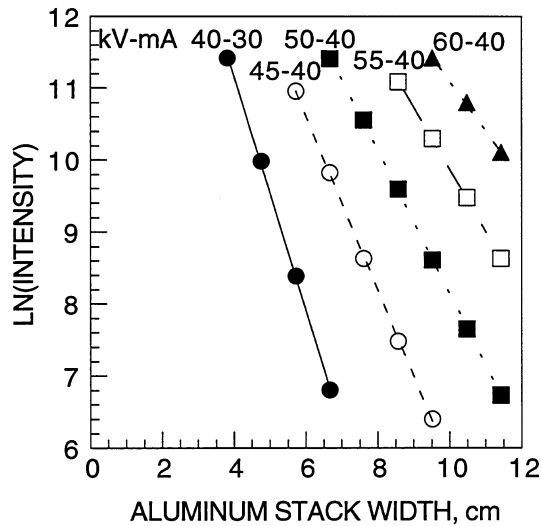


Figure 5-22 X-ray results from scans of aluminum plates.

been scanned before. One might also be interested in knowing the relative magnitude of the incident intensity to compare X-ray measurement techniques with those of other energy sources, such as those using gamma rays. X-ray scans were taken of stacks of aluminum plates to provide data for inferring incident X-ray intensities.

Aluminum plates, each 0.95 cm thick, were stacked side by side starting 8.1 cm from the 0.79 cm diameter X-ray aperture and progressing toward the detector. Stacks of varying thickness were then scanned with the linear X-ray scanner at several voltage and current settings in the ranges 40 to 60 kV and 10 to 40 mA. Scan results at five settings are shown in Figure 5-22. The results were used to extrapolate detector-incident photon intensities of $4\text{E}+07$ to $1\text{E}+08$ counts/sec for these X-ray settings. While the measured X-ray intensities were corrected for the detector dead-time, they were not corrected for pulse pile-up. Incident intensities corrected for pulse pile-up are somewhat greater than the values presented here.

5.3 X-ray Detector Output Characteristics

For semiconductor and NaI scintillation detectors, a photon striking the detector creates an electrical pulse with a pulse area proportional to the photon energy. There is a finite amount of time, called dead-time, needed to process a pulse. Real-time consists of preset live-time during which photons (or pulses) are acquired at the detector and the dead-time required to process those pulses. According to the literature,²⁶ peak throughput of a detector, or photons detected per real-time, is obtained at a %DT (percent dead-time) of 63.2%. This was verified to hold true for the equipment at NIPER by passing X-rays through a core plug in an aluminum coreholder at voltages of 50, 55, and 60 kV and currents of 10 to 40 mA. Results are shown in Figure 5-23. Calculated intensities and throughputs for the coreholder example are shown in Table 5-2. Also shown are the estimated real-times and live-times necessary to obtain 100,000 counts for each %DT.

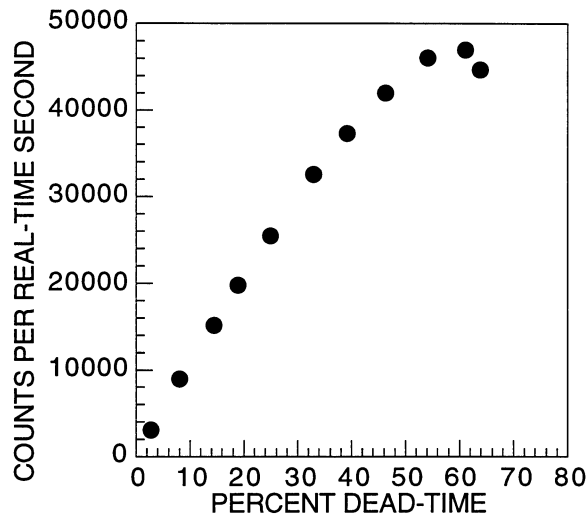


Figure 5-23 Throughput vs. dead-time results for the germanium crystal detector.

The input count rate of a detector is the photon flux uncorrected for detector losses. For high input count rates, pulses are transmitted close together and pile-up, causing lower-energy photons to be summed and interpreted as higher-energy photons. According to the literature, although an absolute photon flux can be calculated by correcting for pulse pile-up and detector efficiency, it is not necessary for comparative measurement of intensities (counts/live-time) if a dead-time of 63.2% is not exceeded.²⁶ This was tested by passing X-rays through a 5 cm thick Berea sandstone slab. Intensities were measured without correcting for pulse pile-up. Aqueous solutions of sodium iodide were placed in a 9.2 mm cuvette in front of the Berea. As can be seen in Figure 5-24, the natural log of the intensity was found to vary linearly with volumetric concentration of sodium iodide in water. Note that the volumetric concentrations of sodium iodide shown correspond to weight concentrations of 0.0, 2.5, 5.0, 7.5, and 10.0%. While linear fits to the data sets of Figure 5-24 all had correlation coefficients better than 0.999, fits with the best correlation coefficients ($R > 0.9995$) occur for cases in which the maximum %DT is less than about 45%.

Table 5-2 Calculated intensity and throughput results for an aluminum coreholder.

Dead-time (DT, fraction)	Live-time (LT, fraction)	Intensity (counts/LT)	Throughput (counts/RT)	RT for 100K (real-time, sec)	LT for 100K (live-time, sec)
0.10	0.90	11728	10555	9.47	8.53
0.20	0.80	25863	20690	4.83	3.87
0.30	0.70	43265	30285	3.30	2.31
0.40	0.60	63933	38360	2.61	1.56
0.50	0.50	87868	43934	2.28	1.14
0.60	0.40	115070	46028	2.17	0.87

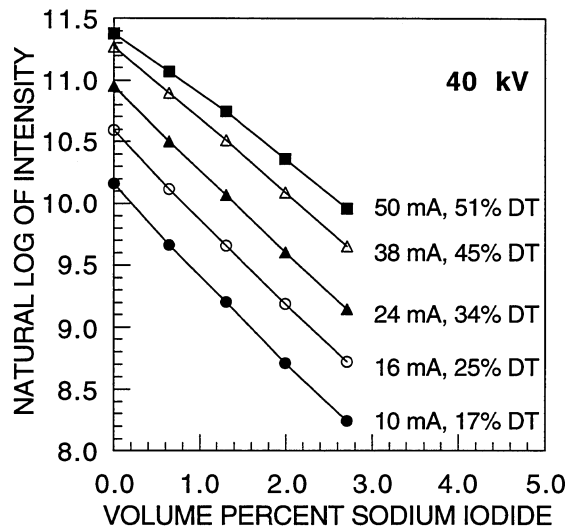


Figure 5-24 Ln (Intensity) vs. NaI concentration for berea sample.

These results indicate X-ray measurements of fluid saturations can be performed using greater X-ray intensities and dead-times than previously practiced at NIPER and still maintain good linearity in the X-ray saturation calibration. Operating at greater intensities reduces the live-time and real-time required to obtain a specified number of counts. This should prove very useful in decreasing the time required to scan a sample while maintaining a high level of accuracy.

5.4 X-Ray Calibrations

X-ray calibrations have sometimes been checked by measurements of changes in X-ray intensities with changes in mass concentration of an X-ray dope as fluids are injected into the rock specimen. Dopes include water or oil soluble compounds containing iodide or bromide. These calibrations are sometimes non-linear. During this reporting period, the non-linearity observed when plotting the natural log of X-ray intensity measurements vs. mass percent of dope was investigated. It was determined that calibrations should not be determined based on mass percent of X-ray dope in the flow stream but rather against volume percent of dope in the flow stream. This is in keeping with Lambert's Law

$$I = I_0 e^{(-k_1 x_1 - k_2 x_2 - \dots)} \quad (4-8)$$

where I is the intensity after radiation of intensity I_0 has passed through materials of thicknesses x_n having linear absorption coefficients k_n .

The volume percent of a salt in a water solution can be determined by analyzing X-ray intensities for different salt concentrations, by knowledge of the brine mass density and by requiring X-ray attenuation by the water to be constant in all cases. The mass density of sodium chloride while in water solution was found to be relatively constant for mass concentrations less than 25%.

Calibrating against several volume percent dope concentrations was found to decrease saturation uncertainty by a factor of five over calibrating against mass percent dope. Calibrating only with the

saturation endpoints (100% doped fluid and 100% non-doped fluid) was found to reduce by a factor of four the uncertainty present when only mass percent dope is considered.

5.5 Low Energy X-ray Scans

Typically, laboratory X-ray measurements of rock fluid saturations are recorded using fairly high X-ray tube voltage and current settings. These are set to produce X-rays with energies sufficient to penetrate metallic coreholders. With these X-ray settings, dopes must be added to one or more of the fluid phases so that the fluids can be distinguished from one another. Low energy X-ray measurements might be suitable for measuring fluid saturations within rock samples with reduced dope concentrations. Ideally, one would like to be able to distinguish fluid saturations without having to dope any of the fluids. Low energy X-ray scans are in progress with rock and fluid samples. These tests are intended to provide information on minimum practical X-ray energies for corefluid saturation measurements and on sample size constraints. The X COM²⁷ computer program is being used as an aid in evaluating X-ray energies below those which can be achieved using the X-ray generator currently used with the X-ray system.

One constraint in using low energy X-ray scans for rock fluid saturation measurements is that the coreholder should not appreciably absorb X-rays. Coreholders fabricated of combinations of carbon fiber and epoxy composites and aluminum are slowly gaining popularity for corefluid applications that require X-ray saturation measurements. The advantage of using a composite coreholder results from the very low X-ray absorption characteristics of the carbon fiber and epoxy resin. Early in the project year, Temco, Inc. of Tulsa, OK allowed NIPER to scan a composite coreholder that they recently fabricated for one of their customers. The X-ray absorption characteristics of the coreholder body were significantly lower than those of any of the titanium and aluminum coreholders that are in the laboratory.

5.6 Composite Coreholder

A composite coreholder was purchased during the project year to facilitate X-ray measurements using low energy scanning techniques. To optimize utility, the coreholder was specified for operating pressures to 55 MPa with temperatures to 130°C. X-ray scans were taken of the coreholder. Scan results revealed that its X-ray absorption characteristics were significantly higher than expected, yielding a product of disappointing qualities for the requirements of the laboratory. Discussions with the manufacturer brought to light that a different aluminum was used for the inner-barrel fabrication compared to what was anticipated. The exact composition of the aluminum was not specified in the purchase requisition. The manufacturer used 2024 aluminum for the inner-barrel fabrication rather than 6061 aluminum to provide better high-temperature strength. The 2024 alloy contains more copper than the 6061 alloy, which yields higher X-ray linear absorption characteristics over the low-energy X-ray spectrum.

Additional analyses, evaluations and discussions with the manufacturer indicated that the coreholder could be optimized with respect to strength, utility, and X-ray absorption characteristics by increasing the inner radius of the aluminum inner-barrel and decreasing the aluminum wall thickness. Machining processes and pressure tests were successfully completed on May 25, 1995, X-ray scans were made of rock plugs within the coreholder under various gas, oil and brine saturation conditions. Results showed that

the coreholder is suitable for tests in which X-ray absorption methods are used to determine two- and three-phase saturations within rock samples during reservoir condition tests. The coreholder will be used for three-phase flow tests with X-ray tube potentials set at from 45 kV to 55 kV. These settings are considerably less than those typically used with X-ray CT scanners.

6.0 EXPLOSION-PROOF OVEN DESIGN

Reservoir fluid flow characteristics are often determined by testing rock core plugs within the laboratory using conditions that mimic those of the petroleum reservoir. For these types of tests, safe methods are required for heating samples. An explosion-proof design to heat a coreflood enclosure to 130°C using a hot silicone-oil circulation system was described in the FY 1994 Topical Report for this project.²⁸ A prototype was built and tested during FY 1995. The enclosure successfully maintained the temperature of an apparatus at 130°C ± 1°C for over 170 hr during a test.

Figure 6-25 is a schematic of a reservoir-condition coreflood apparatus. X-ray scans were required for fluid saturation measurements. A narrow width was required for the flow and heating systems to accommodate the X-ray scanner. An attempt was made to order a heated enclosure from an oven manufacturer. Because of the unique size requirements, the oven manufacturer declined to bid. The heated enclosure had to be designed and built by project staff. The heat system was designed without placing an ignition source within the enclosure. Figure 6-26 is a schematic of the heating system.

The thermostat on the circulation heater did not control the temperature of the circulating oil within acceptable tolerances. A temperature controller was added to the electrical system to provide precise control of power delivered to the circulation heater. The thermostat on the circulation heater is used instead as an over-temperature controller for the oil circulation system. An over-temperature controller was also wired into the electrical system to de-energize the circulation heater if the temperature within the enclosure exceeded a high temperature limit.

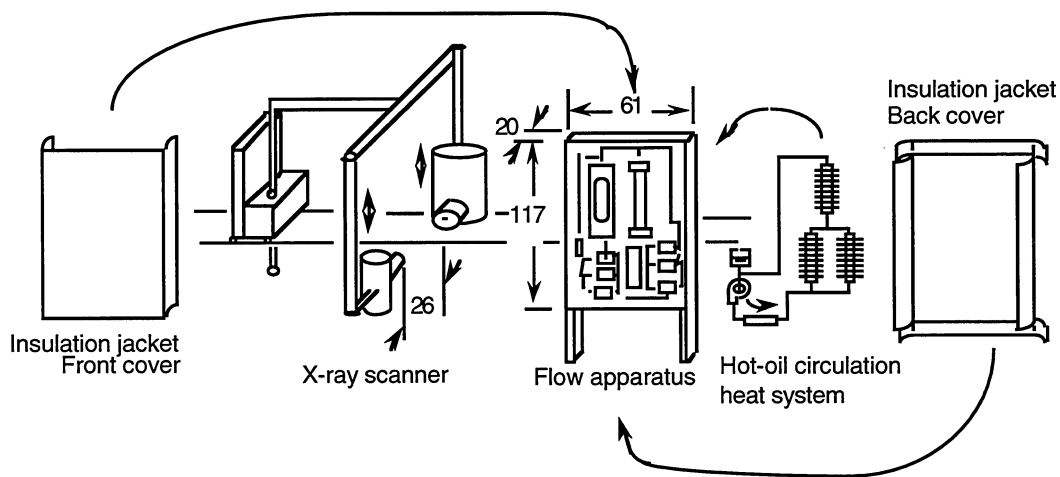


Figure 6-25 Reservoir condition coreflood schematic. Dimensions are in cm.

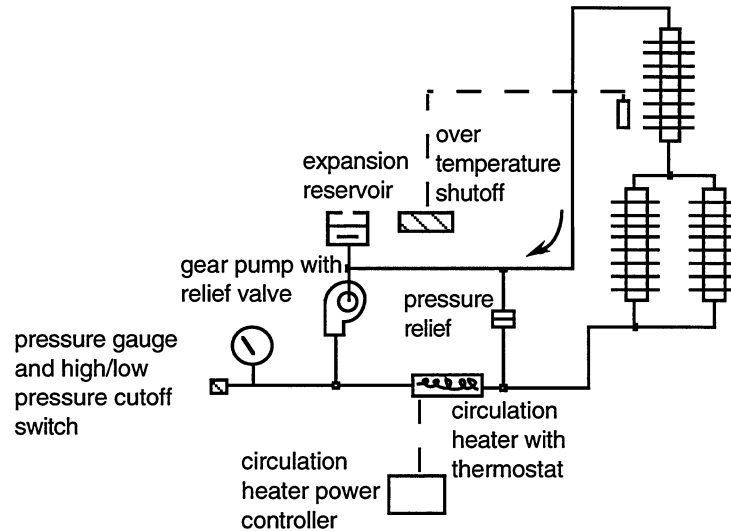


Figure 6-26 Hot oil circulation system

The gear pump which circulates oil through the system is belt driven. The belt drive separates the motor from the hot pump, allowing the pump motor to stay cool during continuous operation. The belt drive also allows the pump to be driven at a lower speed than the motor, which resulted in considerable noise reduction (a similar pump directly coupled to a 1750 rpm motor was so loud that the laboratory staff had to wear earplugs within the lab). The pressure cutoff switch de-energizes the pump if an overpressure condition occurs within the circulation system. Heat is supplied to the coreflow apparatus by the three radiators. Circulation flow lines are insulated to reduce heat-loss from the system.

The system was tested to verify that it could heat the enclosure to a temperature of 130°C. The temperature of the enclosure stabilized to within 1°C of 130°C after about 5 hours when the oil temperature was controlled at 143°C. The enclosure temperature remained constant during a week-long test. This test demonstrated that the hot-oil circulation system is a viable means for heating a coreflow apparatus to reservoir condition tests. A principal advantage of the heating system is that no ignition sources are present within the enclosure. This is especially important for tests with volatile hydrocarbons because the enclosure can be heated without having to use heat transfer devices (electrical resistance heating elements) whose temperatures exceed auto-ignition temperatures of the pressurized hydrocarbons.

7.0 TECHNOLOGY TRANSFER

Members of the project staff participated in numerous technology transfer activities throughout the project year.

Project members provided tours and descriptions of technology to visitors from small independent petroleum consulting and producing companies. The discussions were valuable for discerning what information is typically available to consultants of small independent oil companies for reservoir production designs.

Dan Maloney participated on the Board of Directors of the Society of Core Analysts. Board meetings throughout the year focused the Society technology transfer activities to the core analysis community. Particular emphasis was placed on discussions of the relative permeability workshop which will be held in conjunction with the annual SCA meeting in September, 1995.

Dan Maloney discussed X-ray scanning techniques and reservoir condition special core analysis measurements with staff at the Mobil E&P Technical Center in Dallas. Mr. Maloney also presented a seminar on non-Darcy effects in two-phase flow systems. Research topics of mutual interest were discussed with Mobil staff.

Software to calculate unsteady-state relative permeability and capillary pressure vs. fluid saturation functions from laboratory data measurements was purchased from Doug Ruth, a professor at The University of Manitoba who serves as a consultant to US petroleum laboratories. Professor Ruth provided training on the use of the software to the project staff and gave a seminar at NIPER on core analysis. Project staff discussed relative permeability and capillary pressure phenomena with Dr. Ruth during his visit to NIPER. The discussions were valuable as a bi-directional technology transfer activity.

Dan Maloney discussed core analysis methods with staff of a Tulsa-based core analysis group which provides services for a number of US petroleum companies.

Dan Maloney informally discussed CRADA possibilities with representatives of two major U.S. petroleum companies during the project year. Interest was expressed by both parties.

Discussions with the composite material coreholder manufacturer served as an excellent technology transfer activity. The coreholder manufacturer, who is globally recognized for excellence in manufacturing equipment for petroleum laboratory tests, has a greater appreciation of how to optimize both strength and X-ray absorption characteristics of composite designs for tests that use X-rays or MRI for imaging rock-fluid saturations. The net result is that the manufacturer should be able to enhance the state-of-the-art in composite pressure vessel designs to the benefit of the domestic petroleum industry.

A paper entitled "Consideration of Thermal Effects During Reservoir Condition Special Core Analysis Tests" was completed during this reporting period. The paper is by Dan Maloney and Kevin Doggett of NIPER and James H. Hedges of Phillips Petroleum Company. The paper will be presented at the September 1995 Society of Core Analysts International Symposium.

A presentation describing project objectives and accomplishments was given at the June 25-29, 1995 Bartlesville Project Office Contractor Review Conference.

8.0 OTHER PROJECT ACTIVITIES

A five-year plan for Applied Research in Transmission, Retention, and Distribution of Fluids in Porous Media was completed. An ES&H status report describing environmental, health and safety aspects and evaluations of FY 1995 project work was submitted to the ES&H group at NIPER. Project staff completed pressure vessel training courses during this reporting period on low, intermediate, and high pressure applications. The staff also completed a pressure vessel design course. These courses were held at NIPER by personnel from Lawrence Livermore National Laboratory.

9.0 CONCLUSIONS

In conclusion, significant progress was made toward meeting objectives of providing low cost, simple methods for estimating fluid transmission characteristics of reservoir rocks; improving accuracies of laboratory-measured rock fluid transmission characteristics, and in providing data and descriptions from multiphase fluid flow tests to support coreflood and reservoir simulator developments. The importance of this work is demonstrated by interest from the petroleum industry.

Significant conclusions from this work include the following:

- Comparisons of results from both steady- and unsteady-state techniques indicate that experimental techniques and data analysis methods affect results from both methods.

A combination of the two techniques provides suitable relative permeability results over the entire range of two-phase flow saturations.

- Comparisons of mercury injection capillary pressure results with oil-brine relative permeability results for a number of water-wet rock samples indicate that both follow trends related to permeability magnitude in fairly predictable manners.

This predictability serves as a basis for goals to provide simple correlations among capillary pressure and relative permeability functions.

- Visco-inertial gas flow affects both gas and oil production. It appears that the effects of visco-inertial gas flow on oil production can be treated with a modification to the Forchheimer equation:

$$-dP / dL - [\beta \rho v^2]_{gas} = [\mu v / (k_{eff})]_{oil}$$

- When the gas velocity is sufficiently low, the second term of on the left-hand side of equation becomes negligible, and the equation reduces to the familiar Darcy equation.

When the gas velocity is such that significant visco-inertial resistance results, the second term on the left-hand side of equation accounts for this added flow resistance.

- A prototype explosion-proof oven in which heat is transferred to the coreflood enclosure by hot silicone oil was tested.

The test demonstrated that the hot-oil circulation system is a viable means for heating a coreflood apparatus for reservoir condition tests. A principal advantage of the system is that no ignition sources are present within the enclosure. This is especially important for tests with volatile hydrocarbons because the enclosure can be heated without exceeding the auto-ignition temperatures of the contained hydrocarbons.

10.0 REFERENCES

1. Maloney, D., 1993. *Reservoir-Condition Special Core Analyses and Relative Permeability Measurements on Almond Formation and Fontainebleau Sandstone Rocks*. NIPER-712, (Sept.).
2. Pugh, V., D. Thomas, and S. Gupta. *Correlations of Liquid and Air Permeabilities for Use in Reservoir Engineering Studies*. Paper SCA 9012 presented at the 1990 SCA Annual Technical Conference, Houston, TX, Aug. 14–16, 1990.
3. Jones, S. and W. Roszelle. 1978. *Graphical Techniques for Determining Relative Permeability from Displacement Experiments*. JPT (May) 807–17.
4. Johnson, E., D. Bossler, and V. Neumann, 1959. *Calculation of Relative Permeability from Displacement Experiments*. Petroleum Transactions, AIME, Vol. 216, pp. 370–72.
5. Ruth, D. 1994. *PORTWO Computer program*. Version 6.07. D&B Ruth Enterprises.
6. Craig, F. Jr. 1971. *The Reservoir Engineering Aspects of Waterflooding*. Monograph Series, SPE of AIME, Dallas, 3.
7. Shafer, J., E. Braun, A. Wood III, and J. Wooten. *Obtaining Relative Permeability Data Using A Combination of Steady-State and Unsteady-State Corefloods*. Paper SCA 9009 pres. at the 1990 SCA Conference.
8. Matthews, G., A. Moss, M. Spearing, and F. Voland, 1993. *Network Calculation of Mercury Intrusion Absolute Permeability in Sandstone and Other Porous Media*. Powder Technology, 76, 95–107.
9. Noman, R., N. Shrimanker, and J. Archer, 1985. *Estimation of the Coefficient of Inertial Resistance in High-Rate Gas Wells*. Paper SPE 14207 presented at the 60th Annual Technical Conference and Exhibition of the SPE, Las Vegas, NV, September 22–25.
10. Forchheimer, P. 1901. *Wasserbewegung durch Boden*. ZVDI 45: 1781.
11. Katz, D., et. al. 1959. *Handbook of Natural Gas Engineering*. McGraw Hill Book Co., New York, p. 46.
12. Geertsma, J. 1974. *Estimating the Coefficient of Inertial Resistance in Fluid Flow Through Porous Media*. SPEJ (Oct.) 445.
13. Maloney, D., B. Gall, and C. Raible, 1989. *Non-Darcy Gas Flow Through Propped Fractures: Effects of Partial Saturation, Gel Damage, and Stress*. SPE Production Engineering, November, pp. 417–22.
14. Frederick, D. and R. Graves, 1994. *New Correlations to Predict Non-Darcy Flow Coefficients at Immobile and Mobile Water Saturation*. Paper SPE 28451 presented at the SPE 69th Annual Technical Conference, New Orleans, LA, September 25–28.
15. Holditch, S. and R. Morse, 1976. *The Effects of Non-Darcy Flow on the Behavior of Hydraulically Fractured Gas Wells*. Journal of Petroleum Technology, October, pp. 1169–79.

16. Tek, M., K. Coats, and D. Katz, 1962. *The Effect of Turbulence on Flow of Natural Gas Through Porous Reservoirs*. Journal of Petroleum Technology, July, pp. 799–806.
17. Lee, R., R. Logan, and M. Tek, 1987. *Effect of Turbulence on Transient Flow of Real Gas Through Porous Media*. SPE Formation Evaluation, March, pp. 108–20.
18. Wong, S., 1970. *Effect of Liquid Saturation on Turbulence Factors for Gas-Liquid Systems*. The Journal of Canadian Petroleum Technology, October-December, pp. 274–78.
19. Pursell, D., D. Blakeley, and S. Holditch, 1989. *Discussion of Influence of an Immobile or Mobile Saturation on Non-Darcy Compressible Flow of Real Gases in Propped Fractures*. Journal of Petroleum Technology, December, pp. 1368–69.
20. Evans, R., C. Hudson, and J. Greenlee, 1987. *The Effect of an Immobile Liquid Saturation on the Non-Darcy Flow Coefficient in Porous Media*. SPE Production Engineering, November, pp. 331–38.
21. Evans, E. and R. Evans, 1986. *Influence of an Immobile or Mobile Saturation Upon Non-Darcy Compressible Flow of Real Gases in Propped Fractures*. Paper SPE 15066 presented at the 56th California Regional Meeting of the SPE, Oakland, CA, April 2–4.
22. Cooke, C., 1973. *Conductivity of Fracture Proppants in Multiple Layers*. Journal of Petroleum Technology, September, pp. 1101–7.
23. Noman, R. and J. Archer, 1987. *The Effect of Pore Structure on Non-Darcy Flow in Some Low-Permeability Reservoirs*. Paper SPE/DOE 16400 pres. at the SPE/DOE Low Permeability Reservoirs Symposium, Denver, CO, May 18-19.
24. Dranchuk, P. and L. Kolada, 1968. *Interpretation of Steady Linear Visco-Inertial Gas Flow Data*. The Journal of Canadian Petroleum Technology, Jan-March, pp. 36-40.
25. Gewers, C. and L. Nichol, 1969. *Gas Turbulence Factor in a Microvugular Carbonate*. The Journal of Canadian Petroleum Technology, April-June, pp. 51–6.
26. McBride, J. S. and C. T. Miller, 1994. *Measurements of Phase Fractions in Porous Media by Using X-rays*. Research Report No. ER 4/1.94 Center for Multiphase Research, Department of Environmental Sciences and Engineering, University of North Carolina, Chapel Hill.
27. Berger, M., and J. Hubble, 1987. *X COM: Photon Cross Sections on a Personal Computer*. NBSIR 87-3597, July.
28. Maloney, D. and K. Doggett, 1994. *Relative Permeability Research FY 1994*, Report NIPER/BDM-0067, September.

